Spectrochimica Acta Part A: Molecular and Biomolecular Spectroscopy 223 (2019) 117280

Contents lists available at ScienceDirect

Spectrochimica Acta Part A: Molecular and Biomolecular Spectroscopy

journal homepage: www.elsevier.com/locate/saa

A series of blue-green-yellow-red emitting Cu(I) complexes: Molecular structure and photophysical performance

Liming Zhang [a,*], Qinghui Zuo [b,*]

[a] State Key Laboratory of Luminescence and Applications, Changchun Institute of Optics Fine Mechanics and Physics, Chinese Academy of Sciences, Changchun 130033, PR China
[b] School of Materials Science and Engineering, Changchun University of Science and Technology, No. 7989, Weixing Road, Changchun 130022, PR China

ARTICLE INFO

Article history:
Received 16 April 2019
Received in revised form 14 June 2019
Accepted 15 June 2019
Available online 17 June 2019

Keywords:
Phosphorescent Cu(I)
Molecular structure
Conjugation plane
Frontier molecular orbitals

ABSTRACT

In this work, we designed a series of $[Cu(N—N)(PPh_3)_2]BF_4$ complexes with different optical edge values and emission colors from blue to red, where N—N and PPh_3 denoted a diamine ligand and triphenylphosphine, respectively. Six N—N ligands with various conjugation chains (short π chain, modest π chain and long π chain) were selected. A systematical comparison between these Cu(I) complexes was performed, so that the correlation between N—N structure and $[Cu(N—N)(PPh_3)_2]$ photophysical performance was tentatively discussed. Their single crystal structure was found consistent with literature ones, forming a typical tetrahedral coordination geometry. Density functional theory calculation indicated that their onset electronic transition showed a mixed character of metal-to-ligand-charge-transfer and ligand-to-ligand-charge-transfer. Detailed analysis on photophysical parameters suggested that the absorption edge of $[Cu(N—N)(PPh_3)_2]BF_4$ complex was controlled by conjugation length in diamine ligand. A wide absorption edge needed a short conjugation chain in diamine ligand. Similar tendency was found for their emission spectra. In addition, a long conjugation chain in diamine ligand widened emission spectra obviously. Emission dynamics showed slim correlation with diamine ligand conjugation length since the excited state was controlled mainly by dynamic procedure and steric factor of diamine ligands.

1. Introduction

Luminescent metal complexes have attracted more and more research attention owing to their wide application in optoelectronic devices such as light-emitting panels and solar cells [1–3]. Although heavy metal complexes generally have better performance in aspect of emission variety, emission lifetime and efficiency, more and more concern has been focused on their toxicity and environmental impact [4]. In this case, Cu(I) complexes have been highly recommended owing to their environmental friendliness and economic cost [5–7]. Among them, phosphorescent ones with heteroleptic ligands have been intensively studied. Their ligands include diamine aromatic ligands (N—N) such as 1,10-phenanthroline and phosphorous ligands (P—P) such as PPh_3, forming a representative tetrahedral geometry with molecular formula of $[Cu(N—N)(P—P)]^+$. Such structures have been firstly reported by McMillin in 2002 [5]. Analogous structures have been synthesized and reported since they have shown efficient emission with long-lived emissive center. Feng and his group have performed theoretical calculation on [Cu(N—N)(P—P)] structures [8]. It is reported that their occupied frontier molecular orbitals (FMOs) are composed of Cu (I) d orbital and P—P ligand, which endows these FMOs with dominant metal character. While the unoccupied FMOs are basically the π* of N—N ligands. As a result, the emissive state of [Cu(N—N)(P—P)] structures is generally described as a character of metal-to-ligand-charge-transfer (MLCT).

It is then found that regardless of their intense absorption in UV region, these [Cu(N—N)(P—P)] structures have large Stokes shift and emit low energy emission in yellow region. Detailed analysis on MLCT excited state suggests that there exists an energy-exhausting procedure of structural transformation from tetrahedral geometry (in ground state) to tetragonally flattened geometry (in excited state), leading to decreased energy content and low photoluminescence quantum yield (PLQY) [8]. To control such structural relaxation, Zhang and coworkers incorporated bulky substituents in 2,9-positions of 1,10-phenanthroline [9]. As expected, Stokes shift has been decreased dramatically, and PLQY has been improved greatly. Moreover, Zhang has reported an interesting phenomenon of inner- and inter-molecular π-π stacking which efficiently limits such structural relaxation as well, showing improved PL performance [10]. In the past a few years, continuous efforts have been devoted to reveal the correlation between ligand structure and PL performance. For example, Cabrera and coworkers report a series of [Cu(N—N)(P—P)] structures with MLCT absorption between 400 nm

* Corresponding authors.
E-mail addresses: zhangliming@ciomp.ac.cn (L. Zhang), zuoqinghui@cust.edu.cn (Q. Zuo).

https://doi.org/10.1016/j.saa.2019.117280
1386-1425/

and 450 nm and discuss their HOMO-LUMO energy gaps with DFT methods [11]. Their emission is reported as a mixture of triplet MLCT and triplet LC (ligand-centered) state. Ren and coworkers then present their theoretical work about isomerization and methyl modification to decrease non-radiative decay rate and thus improve emissive performance of triplet MLCT state [12]. Sessolo, Orti and Housecroft have reported ligands of 1,10-phenanthroline and bipyridine substituted at only 2-position, showing red emission with quantum yields of ~38% and emission lifetime of ~10 μs from their [Cu(N—N)(P—P)] complexes [13–15]. Mallick and Sinha have reported phosphino-bridged complexes with MLCT absorption at ~500 nm [16]. Tschierlei and Karnahl have found long-lived excited states in their [Cu(N—N)(P—P)] complexes owing to the extended π-system in anthracene-based diamine ligand [17].

Regardless of these numerous reports, although the key factors affecting MLCT excited state of [Cu(N—N)(P—P)] have been revealed as above stated, high-energy emission, such as deep blue, from [Cu(N—N)(P—P)] structures is still rare [18,19]. This is because their optical edge ($\Delta E = E_{LUMO}$-E_{HOMO}) is usually a narrow one (<450 nm), which technically denies their high energy emission, given the presence of Stokes shift. There is even rare systematical research on how to adjust the ΔE of [Cu(N—N)(P—P)] structures. Given this circumstance, we intend to devote our effort to the correlation between [Cu(N—N)(P—P)] molecular structure and its ΔE. PPh_3 is selected in this work instead of bis(2-diphenylphosphiophenyl)ether since PPh_3 flexible structure avoids π-π stacking and its effect on PL performance. Six N—N ligands with various conjugation chains (short π chain, modest π chain and long π chain) are selected. A systematical comparison between these Cu(I) complexes is performed, so that the correlation between N—N structure and [Cu(N—N)(P—P)] photophysical performance can be tentatively discussed (Scheme 1).

2. Experimental section

2.1. Equipment and reagents

All chemicals were AR grade ones and commercially obtained with no further purifications, including aqueous glyoxal (20%), ammonia, 2-cyanopyridine, sodium azide, 1,10-phenanthroline, 4-(1H-benzo[*d*]imidazol-2-yl)thiazole, ethane-1,2-diamine, benzene-1,2-diamine, 4-methylbenzenesulfonic acid and PPh_3. NMR data were collected on a Varian INOVA 300 spectrometer. Photoluminescence and absorption spectra were recorded using a Hitachi F-7000 spectrometer and a Shimadzu UV-3101 PC spectrophotometer, respectively. Photodynamic data were collected by a FL920 spectrometer equipped with a hydrogen lamp. Photoluminescence quantum yield was determined using the combination of the Hitachi F-7000 spectrometer and an integrating sphere with solid samples. Single crystal data were collected by the combination of a Siemens P4 single-crystal X-ray diffractometer and a Smart CCD-1000 detector (Mo Kα radiation at 298 K). Density functional theory (DFT) calculation was performed on [Cu(N—N)(PPh_3)$_2$] complexes using their single crystal structure as initial geometry. This DFT calculation was performed with Firefly in vacuum at RB3LYP/SBKJC level. Graphical plotting for frontier molecular orbitals was done by wxMacmolplt software package (contour value = 0.03).

2.2. Synthesis of N—N ligands

L1A. 1H,1′H-2,2′-biimidazole (L1A) was obtained following below procedure [20]. Aqueous glyoxal (20%) was placed in water bath at 45 °C, then ammonia was bubbled into this solution for 2 h. The mixture was further stirred overnight. Solid product was collected, washed with water and then dissolved in ethylene glucol. After being decolorized by C powder, the solution was cooled. White solid product was obtained as L1A. ^{1}H NMR (DMSO d_6): δ 7.08 (s).

L1B. 2-(1H-tetrazol-5-yl)pyridine (L1B) was obtained as follows. A mixture of 2-cyanopyridine (10 mmol), NaN_3 (15 mmol), ZnBr (10 mmol) and water (30 mL) was prepared and heated at 100 °C for 8 h. After cooling, solid NaOH (25 mmol) was added. The solution was filtered and then mixed with HCl until pH = 1. Crude product was collected and purified on a silica gel column to give L1B as white solid. ^{1}H NMR ($CDCl_3$): δ 8.21 (1H, t), 8.25 (1H, t), 8.33 (1H, d, J = 6.0), 8.85 (1H, d, J = 3.6).

L2A. 4-(1H-benzo[*d*]imidazol-2-yl)thiazole (L2A) was purchased and used as received as above mentioned.

L2B. 2-phenyl-5-(pyridin-2-yl)-1,3,4-oxadiazole (L2B) was obtained as follows. A mixture of L1B (10 mmol), benzoyl chloride (15 mmol)

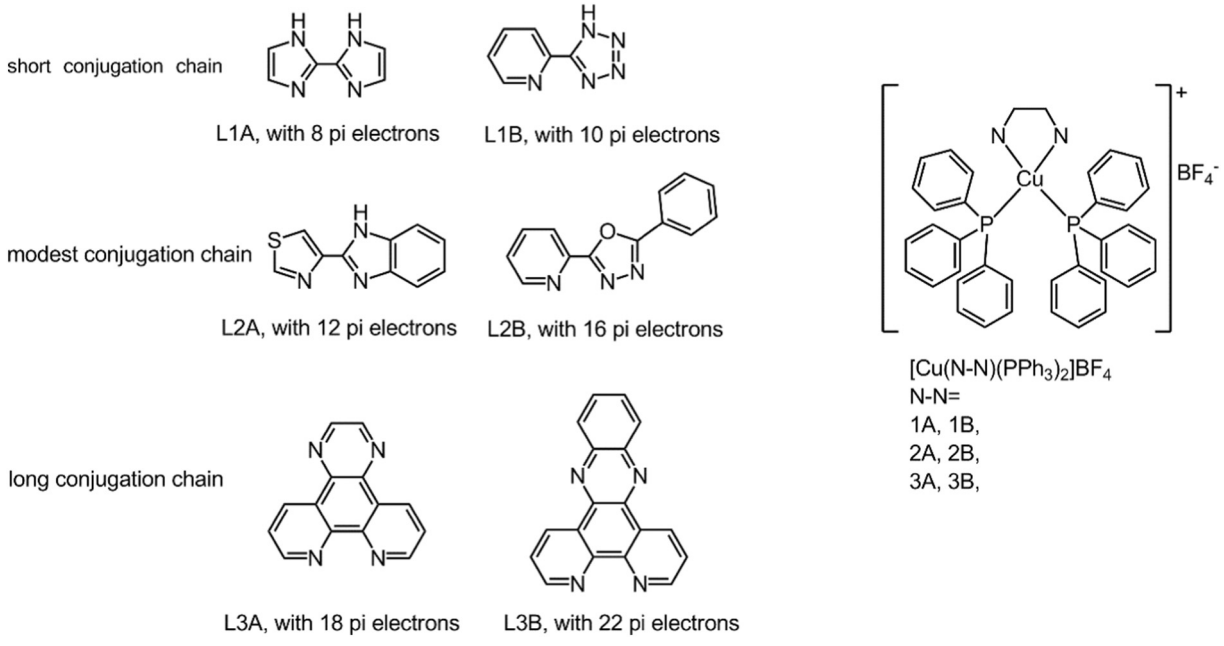

Scheme 1. Molecular structure of [Cu(N—N)(PPh_3)$_2$]BF_4 complexes used in this work.

and 35 mL of pyridine was prepared and stirred under N_2 atmosphere at 120 °C for 2 days. After cooling, crushed ice was added. Crude product was collected and purified on a silica gel column to give L2B as white powder. ^{1}HNMR ($CDCl_3$): δ 7.45 (1H, m), 7.57 (3H, m), 7.91 (1H, m), 8.22 (1H, t), 8.28 (1H, t), 8.35 (1H, d, $J = 6.0$), 8.84 (1H, d, $J = 3.6$).

L3A. 1,10-phenanthroline-5,6-dione (Phen-O) was firstly prepared following a literature procedure [21]. Then a mixture of Phen-O (10 mmol), ethane-1,2-diamine (3 mL), ethanol (25 mL) and 4-methylbenzenesulfonic acid (1 mmol) was prepared and stirred at 80 °C overnight. Crude product was collected, washed with ethanol and purified in hot ethanol to give L3A as white powder. ^{1}H NMR ($CDCl_3$): δ7.81(m, 2H), 9.02 (s, 2H), 9.33(d, 2H, $J = 8.0$ Hz), 9.53(d, 2H, $J = 8.0$ Hz).

L3B. Dipyrido[3,2-a:2′,3′-c]phenazine (L3B) was synthesized following a similar procedure to L3A, except that ethane-1,2-diamine was replaced with benzene-1,2-diamine in this run. ^{1}H NMR ($CDCl_3$): δ, 7.81 (m, 2H), 7.94 (d, 2H, $J = 6.4$ Hz), 8.32 (d, 2H, $J = 6.4$ Hz), 9.24 (d, 2H, $J = 8.0$ Hz), 9.61 (d, 2H, $J = 8.0$ Hz).

2.3. Synthesis of [Cu(N—N)(PPh_3)$_2$] complexes

All [Cu(N—N)(PPh_3)$_2$] complexes were synthesized following a classical procedure [19]. Their identity was confirmed by NMR, elemental analysis and single crystal analysis. These single crystals were used for later characterization, including photophysical analysis.

[Cu(L1A)(PPh_3)$_2$]BF_4. Starting compound [Cu(CH_3CN)$_4$]BF_4 was prepared as follows. A mixture of [Cu(CH_3CN)$_4$]BF_4 (5 mmol), PPh_3 (10 mmol) and $CHCl_3$ (10 mL) was prepared and stirred for 30 min under ambient condition. Then L1A (5 mmol) was added. The resulting solution was stirred for another 60 min. 5 mL of ethanol was added, then this solution was filtered. The natural evaporation of solvent gave bulk solid. ^{1}H NMR($CDCl_3$): δ 8.05 (t, 2H), 7.97 (t, 2H), 7.35 (t, 11H), 7.26 (m, 4H), 7.23 (m, 4H), 7.05 (m, 8H), 6.60 (m, 3H). Elemental analysis for $C_{42}H_{36}B_1Cu_1F_4N_2P_2$: C, 62.35, H, 4.48, N, 6.92. Found: C, 62.27, H, 4.56, N, 6.84.

[Cu(L1B)(PPh_3)$_2$]BF_4. Its synthetic procedure was similar to [Cu(L1A)(PPh_3)$_2$]BF_4, except that L1A was replaced by L1B in this run. ^{1}H NMR($CDCl_3$): δ 8.18 (d, 2H), 8.03 (t, 2H), 7.36 (t, 11H), 7.28 (m, 4H), 7.25 (m, 4H), 7.07 (m, 8H), 6.62 (m, 3H). Elemental analysis for $C_{42}H_{35}B_1Cu_1F_4N_5P_2$: C, 61.36, H, 4.29, N, 8.52. Found: C, 61.24, H, 4.44, N, 8.47.

[Cu(L2A)(PPh_3)$_2$]BF_4. Its synthetic procedure was similar to [Cu(L1A)(PPh_3)$_2$]BF_4, except that L1A was replaced by L2A in this run. ^{1}H NMR($CDCl_3$): δ 7.98–7.94 (m, 4H), 7.62–7.58 (m, 2H), 7.37 (t, 11H), 7.29 (m, 4H), 7.24 (m, 4H), 7.02 (m, 8H), 6.59 (m, 3H). Elemental analysis for $C_{46}H_{37}B_1Cu_1F_4N_3P_2S_1$: C, 63.06, H, 4.26, N, 4.80. Found: C, 62.95, H, 4.35, N, 4.71.

[Cu(L2B)(PPh_3)$_2$]BF_4. Its synthetic procedure was similar to [Cu(L1A)(PPh_3)$_2$]BF_4, except that L1A was replaced by L2B in this run. ^{1}H NMR($CDCl_3$): δ 8.02–7.98 (m, 4H), 7.36–7.28 (m, 13H), 7.25 (m, 4H), 7.21 (m, 4H), 7.01 (m, 8H), 6.60 (m, 3H). Elemental analysis for $C_{49}H_{39}B_1Cu_1F_4N_3P_2O_1$: C, 65.53, H, 4.38, N, 4.68. Found: C, 65.57, H, 4.42, N, 4.73.

[Cu(L3A)(PPh_3)$_2$]BF_4. Its synthetic procedure was similar to [Cu(L1A)(PPh_3)$_2$]BF_4, except that L1A was replaced by L3A in this run. ^{1}H NMR($CDCl_3$): δ 9.13 (d, 2H), 9.01 (d, 2H), 8.81 (m, 2H), 7.75 (m, 2H), 7.33 (t, 11H), 7.23 (m, 4H), 7.16 (m, 4H), 7.04 (m, 8H), 6.63 (m, 3H). Elemental analysis for $C_{50}H_{38}B_1Cu_1F_4N_2P_2$: C, 66.20, H, 4.22, N, 6.18. Found: C, 66.27, H, 4.31, N, 6.15.

[Cu(L3B)(PPh_3)$_2$]BF_4. Its synthetic procedure was similar to [Cu(L1A)(PPh_3)$_2$]BF_4, except that L1A was replaced by L3B in this run. ^{1}H NMR($CDCl_3$): δ9.24 (d, 2H), 9.11 (d, 2H), 8.04 (d, 2H), 7.74 (d, 2H), 7.60 (m, 2H), 7.34 (t, 11H), 7.25 (m, 4H), 7.21 (m, 4H), 7.03 (m, 8H), 6.60 (m, 3H). Elemental analysis for $C_{54}H_{40}B_1Cu_1F_4N_2P_2$: C, 67.76, H, 4.21, N, 5.85. Found: C, 67.83, H, 4.33, N, 5.79.

3. Result and discussion

3.1. Molecular structure

For a clear understanding on the design strategy of this work, a detailed explanation is given as follows. As above mentioned, although bis(2-diphenylphosphinophenyl)ether (POP) is a widely used auxiliary phosphorous ligand for [Cu(N—N)(P—P)] complexes, its phenyl rings are restricted by its O atom and close to N—N ligand, resulting in inner-molecular π-π stacking which affects PL performance of [Cu(N—N)(POP)] complexes. To eliminate such effect, PPh_3 is selected as the auxiliary ligand in this work since the free rotation of its phenyl rings compromises such highly ordered π-π stacking. As for the six diamine ligands, they are all coplanar ones with similar coordination performance. There are electron-donors or electron-acceptors in these coplanar π chains. They are divided into three groups according to the number of their conjugation π electrons, so that the correlation between the optical edge of [Cu(N—N)(PPh_3)$_2$]BF_4 and N—N ligand structure can be discussed.

Owing to the rigid coplanar diamine ligands, [Cu(N—N)(PPh_3)$_2$]BF_4 complexes tend to crystalize in solid state. Fig. 1 shows their ORTEP plotting, corresponding key structural parameters are listed in Table 1. It is clear that these [Cu(N—N)(PPh_3)$_2$]BF_4 complexes all adopt a similar coordination geometry to literature cases [8]. Two N atoms from a N—N ligand and two P atoms from two PPh_3 ligands coordinate with a Cu(I) center, forming a typical tetrahedral coordination geometry. This geometry is slightly distorted owing to its heterogeneous ligands, as suggested by their structural parameters. All Cu—P bonds are quite similar to each other owing to their identical coordination P atom. The Cu—N bonds, however, are slightly different from each other but still comparable to literature ones [8]. It is found that the Cu—N bond between Cu(I) and the N atom from a five-membered ring (imidazole etc., >2.1 Å) is longer than that between Cu(I) and the N atom from a six-membered ring (pyridine etc., <2.1 Å). This tendency is independent of electron-donors or acceptors in diamine ligands. We thus attribute its causation to the strong coordination tension in a five-membered ring [20]. Coordination bite angles of N-Cu-N (<80°) are typically smaller than literature values (>80°). In addition, P-Cu-P bite angles vary in a wide region ranging from 118° to 126°. This fact actually means a crowded coordination environment, and both diamine ligand and PPh_3 ligand try to decrease coordination hindrance by leaving the Cu(I) center.

Regardless of the close distance between aromatic rings in these [Cu(N—N)(PPh_3)$_2$]BF_4 complexes, no obvious inner-molecular and intermolecular π-π stacking is observed, as above expected. This is because the highly ordered π-π stacking involves the re-arrangement and orientation adjustment of aromatic rings. These [Cu(N—N)(PPh_3)$_2$]BF_4 complexes cannot satisfy this requirement owing to the free rotation of phenyl rings in PPh_3 ligand. The absence of such π-π stacking ensures that MLCT excited state performance is controlled by diamine ligand electronic structure solo, with neglectable geometric factor to be considered.

3.2. FMO analysis by DFT

Feng's work suggests that, unlike Zn(II) complexes, for most [Cu(N—N)(P—P)] complexes, Cu(I) d orbitals contribute to FMO obviously and participate in their MLCT photophysical procedures [8]. For a confirmation on the MLCT nature in our [Cu(N—N)(PPh_3)$_2$]BF_4 complexes, a DFT (density functional theory) calculation is performed on their crystal structures. Fig. 2 shows graphic presentation of their HOMO (the highest occupied molecular orbital) and LUMO (the lowest unoccupied molecular orbital). Their energy levels and transition energy values are listed in Table 2. It is clear that the occupied FMOs have mixed character with contribution from Cu(I) center and the P atom of PPh_3 ligand. As for the unoccupied FMOs, they are completely composed of diamine

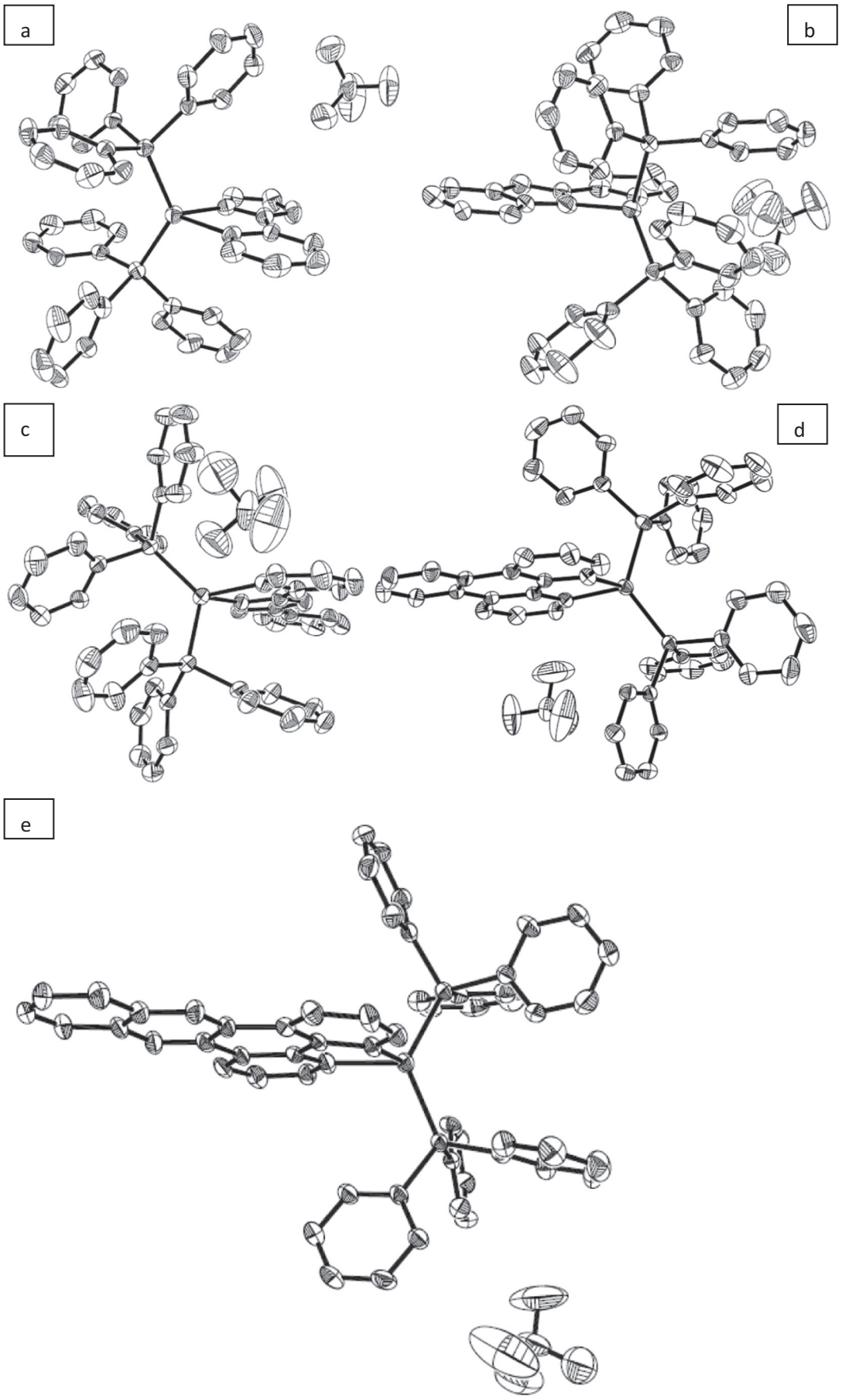

Fig. 1. ORTEP plotting of $[Cu(N—N)(PPh_3)_2]BF_4$ complexes, a, $[Cu(L1B)(PPh_3)_2]BF_4$, b, $[Cu(L2A)(PPh_3)_2]BF_4$, c, $[Cu(L2B)(PPh_3)_2]BF_4$, d, $[Cu(L3A)(PPh_3)_2]BF_4$, e, $[Cu(L3B)(PPh_3)_2]BF_4$. H atoms were not plotted for clarity.

Table 1
Selected geometric parameters of $[Cu(N—N)(PPh_3)_2]BF_4$ complexes.

	N-N=				
	L1B	L2A	L2B	L3A	L3B
Bond length (Å)					
Cu(1)-N(1)	2.186	2.157	2.154	2.068	2.105
Cu(1)-N(2)	2.103	2.042	2.095	2.083	2.069
Cu(1)-P(1)	2.258	2.229	2.278	2.237	2.272
Cu(1)-P(2)	2.254	2.281	2.237	2.249	2.275
Bond angle (°)					
N(1)-Cu-N(2)	78.15	79.04	78.47	80.22	79.36
N(1)-Cu-P(1)	114.15	125.70	100.37	119.87	111.23
N(2)-Cu-P(1)	103.40	119.17	109.33	108.93	108.62
N(1)-Cu-P(2)	110.71	107.99	121.63	108.93	111.15
N(2)-Cu-P(2)	112.65	106.38	117.69	117.00	113.59
P(1)-Cu-P(2)	126.75	118.19	120.96	120.63	124.09

ligands π*. The onset electronic transitions between occupied FMOs and unoccupied ones are thus endowed with a mixed character of MLCT (metal-to-ligand-charge-transfer) and LLCT (ligand-to-ligand-charge-transfer). This conclusion is consistent with literature reports on similar Cu(I) complexes [22]. Such kind of excited state (MLCT&LLCT), especially MLCT one, generally suffers from a structural relaxation from tetrahedral geometry to tetragonally flattened geometry, accompanied by non-radiative decay. As a consequence, excited state energy is decreased and quenched, leading to low emission efficiency and low-energy emission (large Stokes shift) [9,10]. This statement will be further discussed below.

It is still noticed that the energy levels of occupied FMOs are usually localized in a narrow region (−8.47 eV to −8.31 eV for HOMO-1, −8.22 eV to −7.96 eV for HOMO). On the other hand, those of unoccupied FMOs vary in a wide region (−5.22 eV to −4.33 eV for LUMO, −4.52 eV to −3.65 eV for LUMO+1). This is well explained by their nature. Since occupied FMOs have dominant Cu(I) contribution, their energy levels are thus limited in a fixed region, despite of different diamine ligands and their slim contribution. As for the unoccupied FMOs, they are diamine ligand π* orbitals in nature, which endows them with a great variety. It is still observed that electron-donors with lone pairs in diamine ligand, such as the S atom in L2A ligand, lead to obvious increase of both HOMO and LUMO energy levels. Correspondingly, onset electronic transition energy is increased. While, a long conjugation chain, such as L3A and L3B ligands, tends to decrease HOMO and LUMO energy levels. In addition, electron-acceptors tend to decrease both HOMO and LUMO energy levels as well, such as L1B ligand, but its short conjugation chain compromises such decrease effect.

Table 2
Energy levels and transition energy values of $[Cu(N—N)(PPh_3)_2]BF_4$ complexes.

	N-N=				
Energy (eV)	L1B	L2A	L2B	L3A	L3B
LUMO+1	−4.41	−3.65	−3.97	−4.59	−4.52
LUMO	−5.22	−4.33	−4.92	−4.77	−4.91
HOMO	−8.22	−7.63	−8.04	−7.96	−8.00
HOMO-1	−8.47	−8.14	−8.48	−8.46	−8.31
$S_0 \rightarrow S_1$	2.42	2.62	2.55	2.65	2.63
$S_0 \rightarrow S_2$	2.49	3.08	2.77	2.84	2.82

Based on this analysis, it is found that there are two dominant factors for a diamine ligand in affecting the energy levels of these $[Cu(N—N)(PPh_3)_2]BF_4$ complexes: (1) the length of conjugation chain and (2) electron donors or acceptors in conjugation chain. Their effect is briefed as follows. A long conjugation chain decreases HOMO and LUMO energy levels along with onset electronic transition energy, while a short one does otherwise. Electron donors in conjugation chain increases HOMO and LUMO energy levels, along with onset electronic transition energy, while electron acceptors do otherwise. This hypothesis is firstly confirmed by the DFT result shown in Table 2 and will be further confirmed by below discussion.

3.3. Absorption spectra

The onset electronic transition corresponds to an absorption edge. In this case, absorption spectra of these $[Cu(N—N)(PPh_3)_2]BF_4$ complexes are recorded and shown in Fig. 3. Similar to literature case, each absorption spectrum of these $[Cu(N—N)(PPh_3)_2]BF_4$ complexes consists of two major sections, a strong absorption in high energy UV region from 230 nm to 330 nm and a weak absorption in low energy region from 350 nm to ~450 nm. The strong absorption peaks have been revealed by DFT calculation result as π → π* transition of diamine and phosphorous ligands [8,18]. As for the weak absorption band, no such absorption band is observed from diamine or phosphorous ligands. It is thus named as the electronic transition of MLCT&LLCT, as above mentioned [8]. Corresponding absorption edge (λ_{abs}) data are summarized in Table 3 for comparison convenience. It is obvious that the optical edge values of the first three $[Cu(N—N)(PPh_3)_2]BF_4$ complexes (>405 nm) are much higher than those of literature reports (<450 nm) [8,9,23]. These high absorption edge values guarantee their high energy emission, which will be confirmed below. It is clear that λ_{abs} follows an obvious order of $[Cu(L1A)(PPh_3)_2]BF_4$ (366 nm) < $[Cu(L1B)(PPh_3)_2]BF_4$ (401 nm) < $[Cu(L2A)(PPh_3)_2]BF_4$ (405 nm) < $[Cu(L2B)(PPh_3)_2]BF_4$ (448 nm) < $[Cu(L3A)(PPh_3)_2]BF_4$ (460 nm) < $[Cu(L3B)(PPh_3)_2]BF_4$ (466 nm). This

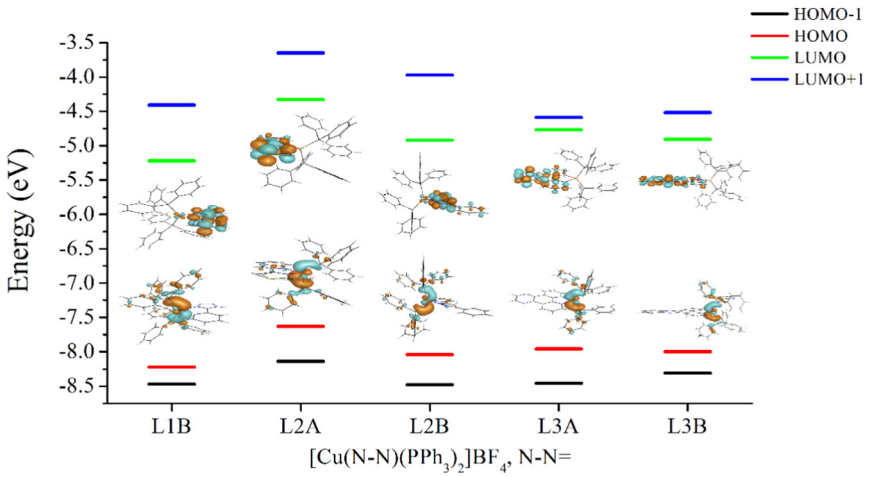

Fig. 2. Graphic presentation for HOMO and LUMO, and energy levels of FMOs.

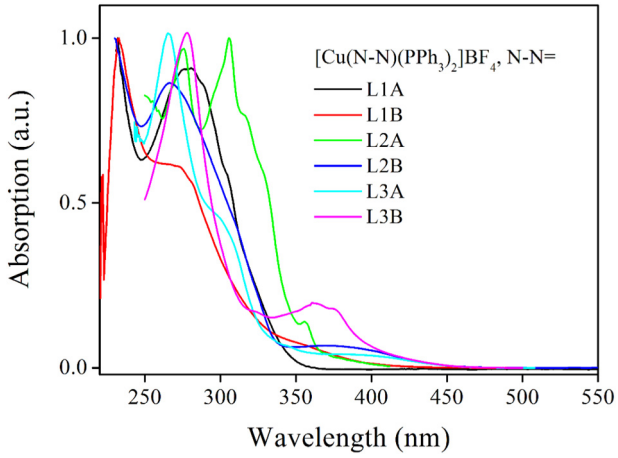

Fig. 3. Absorption spectra of $[Cu(N—N)(PPh_3)_2]BF_4$ complexes in CH_2Cl_2 solution with concentration of 1 μM.

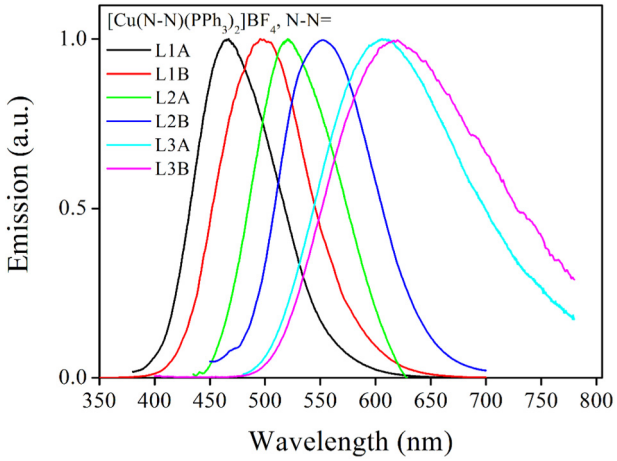

Fig. 4. Emission spectra of $[Cu(N—N)(PPh_3)_2]BF_4$ complexes in solid state.

order perfectly matches the order of π electron number of their diamine ligands, L1A (8) < L1B (10) < L2A (12) < L2B (16) < L3A (18) < L3B (22), which can be explained as follows. As revealed by DFT calculation result of this work and literature reports, HOMO of $[Cu(N—N)(PPh_3)_2]BF_4$ complexes is mainly composed of Cu(I) orbitals and the P atom from PPh_3 ligand [8]. There is rather slim contribution from N—N ligand. The HOMO energy level is thus restricted in a narrow region. As for LUMO, it is diamine ligand π* orbital in nature. In other words, LUMO energy level is variable and controlled just by diamine structure (π*). In this case, the absorption edge between HOMO and LUMO is actually controlled by diamine ligand (π*). A short conjugation chain in diamine ligand leads to a high level π* of this diamine ligand, and consequently a wide absorption edge of its $[Cu(N—N)(PPh_3)_2]BF_4$ complex. Given a diamine ligand with a longer conjugation chain, more π electrons are introduced, which decreases π* energy level of this diamine ligand and consequently the absorption edge of its $[Cu(N—N)(PPh_3)_2]BF_4$ complex. It is thus concluded that the absorption edge of $[Cu(N—N)(PPh_3)_2]BF_4$ complex is controlled by diamine conjugation length. A wide absorption edge needs a short conjugation chain in diamine ligand.

3.4. Emission spectra

Upon photoexcitation on their MLCT&LLCT state, bright emission is observed for all these $[Cu(N—N)(PPh_3)_2]BF_4$ complexes. As shown in Fig. 4, each complex shows a broad emission band. Various emission colors from blue to red is observed from these $[Cu(N—N)(PPh_3)_2]BF_4$ complexes. There are no vibronic details or shoulder peaks, indicating that the excited state has a charge transfer character. This conclusion is reasonable since its emissive state is originated from MLCT&LLCT excited state [8]. Interestingly, the emission peak of these $[Cu(N—N)(PPh_3)_2]BF_4$ complexes follows the same order of their absorption edge, $[Cu(L1A)(PPh_3)_2]BF_4$ (466 nm) < $[Cu(L1B)(PPh_3)_2]BF_4$ (499 nm) < $[Cu(L2A)(PPh_3)_2]BF_4$ (522 nm) < $[Cu(L2B)(PPh_3)_2]BF_4$ (553 nm) < $[Cu(L3A)(PPh_3)_2]BF_4$ (607 nm) < $[Cu(L3B)(PPh_3)_2]BF_4$ (620 nm). This fact tentatively suggests that the emission energy of $[Cu(N—N)(PPh_3)_2]BF_4$ complexes is mainly controlled by their intrinsic energy gap between HOMO and LUMO. Steric factors, such as incorporating bulky substituents into 2,9-positions of 1,10-phenanthroline, only minimize the energy loss of MLCT excited state, but fail to increase or even control the energy content of MLCT excited state.

For comparison convenience, Stokes shift between absorption edge and emission peak of each $[Cu(N—N)(PPh_3)_2]BF_4$ complex is listed in Table 3. FWHM (full-width-at-half-maximum) values are given in Table 3 as well. It is clear that all these $[Cu(N—N)(PPh_3)_2]BF_4$ complexes have large Stokes shift values. This is because their MLCT&LLCT excited state tends to experience a structural relaxation from tetrahedral geometry to tetragonally flattened geometry before reaching the lowest emissive S_1 state [8]. In generally, a short conjugation chain has a minimal steric hindrance to stop such structural relaxation, which is consistent with the highest Stokes shift value of $Cu(L1A)(PPh_3)_2]BF_4$ (0.727 eV). Upon a longer conjugation chain, its steric hindrance is increased, leading to decreased Stokes shift values of the other five $[Cu(N—N)(PPh_3)_2]BF_4$ complexes. As for FWHM values, a similar order is found, $[Cu(L1A)(PPh_3)_2]BF_4$ (86 nm) < $[Cu(L2A)(PPh_3)_2]BF_4$ (90 nm) < $[Cu(L1B)(PPh_3)_2]BF_4$ (93 nm) < $[Cu(L2B)(PPh_3)_2]BF_4$ (96 nm) < $[Cu(L3A)(PPh_3)_2]BF_4$ (156 nm) < $[Cu(L3B)(PPh_3)_2]BF_4$ (177 nm). It seems that a short conjugation chain in diamine ligand leads to a narrow emission band, while a long one in diamine ligand widens emission band greatly. This tendency is even more obvious in $[Cu(L3A)(PPh_3)_2]BF_4$ and $[Cu(L3B)(PPh_3)_2]BF_4$, considering their large FWHM values. This is because excited electrons are mainly localized on π* orbitals of diamine ligands. A short conjugation chain in diamine ligand means a restricted distribution of excited state electrons. On the other hand, a long one leads to a broad distribution of these excited state electrons, resulting in multiple sublevels, which consequently gives a broad emission band.

Table 3
Photophysical parameters of $[Cu(N—N)(PPh_3)_2]BF_4$ complexes in CH_2Cl_2 solution or in solid state.

	N-N=					
	L1A	L1B	L2A	L2B	L3A	L3B
Number of π electrons	8	10	12	16	18	22
[a]λ_{abs} (nm)	366	401	405	448	460	466
[b]λ_{em} (nm)	466	499	522	553	607	620
Stokes shift (eV)	0.727	0.607	0.686	0.526	0.653	0.661
FWHM (nm)	86	93	90	96	156	177
τ_1 (μs)	1.638	1.615	13.211	12.179	5.907	5.868
τ_2 (μs)	8.366	6.210	71.089	121.530	5.908	88.751
τ (μs)	6.873	5.212	66.711	107.448	5.907	70.285
Φ	0.10	0.22	0.17	0.59	0.23	0.27
K_r ($\times 10^3$ S^{-1})	14.455	42.210	2.548	5.491	38.935	3.841
K_{nr} ($\times 10^3$ S^{-1})	130.941	149.655	12.442	3.816	130.346	10.386

[a] Absorption edge.
[b] Emission peak.

3.5. Lifetime and PLQY

For a better understanding on the excited state of these $[Cu(N—N)(PPh_3)_2]BF_4$ complexes, their emission decay dynamics are recorded and shown in Fig. 5. Detailed fitting parameters are listed in Table 3. It is observed that all six $[Cu(N—N)(PPh_3)_2]BF_4$ complexes follow biexponential decay mode with two long-lived decay centers (τ_1 and τ_2). Their lifetimes are obviously different from each other, regardless

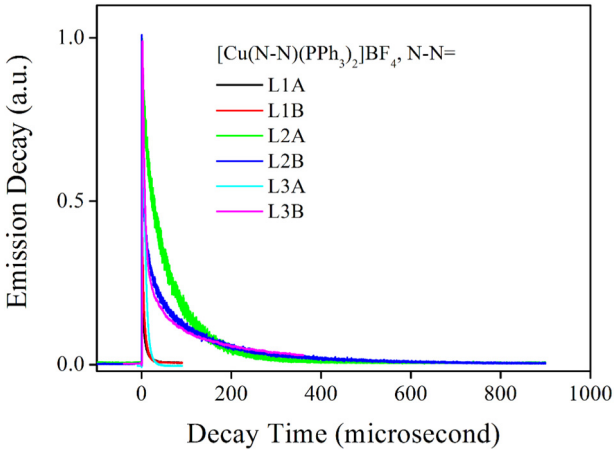

Fig. 5. Emission decay dynamics of $[Cu(N—N)(PPh_3)_2]BF_4$ complexes in solid state.

of their microsecond scale. This observation is consistent with the mixture of MLCT&LLCT in excited state. Their mean lifetime (τ) values listed in Table 3 suggest that their emission has a triplet nature. As a consequence, the emissive center of these $[Cu(N—N)(PPh_3)_2]BF_4$ complexes can be named as triplet MLCT&LLCT, which is consistent with literature case [8]. It has been above mentioned that there is strong $\pi \rightarrow \pi^*$ absorption in each $[Cu(N—N)(PPh_3)_2]BF_4$ complex. Generally, in an emissive center with biexponential decay behavior, there exists a potential surface crossing from $\pi \rightarrow \pi^*$ sate (localized at higher energy region) to MLCT state (localized at lower energy region) [23]. In this case, the short-lived emissive center τ_1 is named as the radiative decay of $\pi \rightarrow \pi^*$ excited sate, while the long-lived emissive center τ_2 is named the radiative decay of MLCT excited state.

Photoluminescence quantum yields (PLQYs, Φ) of these $[Cu(N—N)(PPh_3)_2]BF_4$ complexes are measured and listed in Table 3. No surprise, similar to the case of Stokes shift, $[Cu(L1A)(PPh_3)_2]BF_4$ has the lowest PLQY owing to its intense structural relaxation. As for the other $[Cu(N—N)(PPh_3)_2]BF_4$ complexes, their diamine ligands offer additional steric hindrance, leading to decreased structural relaxation in excited state and consequently increased PLQYs. For example, it is observed that the PLQY of $[Cu(L2B)(PPh_3)_2]BF_4$ is higher than those of other $[Cu(N—N)(PPh_3)_2]BF_4$ complexes obviously. This observation may be explained by the large rigid coplanar structure in L2B ligand. There may be even inner- or inter-molecular stacking in $[Cu(L2B)(PPh_3)_2]BF_4$, which effectively limits its structural relaxation and results in a high PLQY value [10].

For a better understanding on the radiative and non-radiative decay procedures in $[Cu(N—N)(PPh_3)_2]BF_4$ complexes, their decay probability values (K_r and K_{nr}) are calculated with Formula (1) and Formula (2).

$$\Phi = \frac{k_r}{k_r + k_{nr}} \quad (1)$$

$$\frac{1}{\tau} = k_r + k_{nr} \quad (2)$$

With their PLQY and τ values on hand, corresponding decay probability values are calculated and listed in Table 3. It is observed that K_r varies in a wide region from $2.548 \times 10^3\ S^{-1}$ to $42.210 \times 10^3\ S^{-1}$. There is, however, no obvious correlation between K_r and conjugation chain length. The existence of electron donor or acceptor exerts no direct influence on K_r as well. This is because the emissive decay of triplet MLCT&LLCT is actually controlled by a dynamic procedure of the lowest emissive state and the potential surface crossing from $\pi \rightarrow \pi^*$ sate to MLCT state. This procedure has little effect with the energy level of diamine ligand. As for K_{nr}, its value depends on the geometric structure of diamine ligand greatly. Generally, a small diamine ligand with a short conjugation chain offers a high K_{nr} value, while a large diamine ligand with a long conjugation chain tends to present a low K_{nr} value. This is because the non-radiative decay procedure of MLCT&LLCT excited state is mainly dominated by its structural relaxation, as above mentioned. Here, steric factor plays an important role. Be more specific, a small ligand offers limited steric hindrance to stop the structural relaxation, so that an intense geometric relaxation is occurred, leading to a high K_{nr} value. On the other hand, a large ligand with obvious steric hindrance and rigid structure may restrict such geometric relaxation, decreasing K_{nr} value. It is thus concluded that the PL performance of $[Cu(N—N)(PPh_3)_2]BF_4$ complexes is mainly controlled by dynamic procedure and steric factor of diamine ligands. No direct correlation is found with diamine ligand conjugation length.

4. Conclusion

To sum up, this paper presented six $[Cu(N—N)(PPh_3)_2]$ complexes with various absorption edge values and emission colors from blue to red. Their six diamine ligands were divided into three groups (short conjugation chain, modest conjugation chain and long conjugation chain) by the number of their π electrons. Their single crystals were firstly obtained and discussed. It was found that these complexes all adopted a typical tetrahedral coordination geometry. DFT calculation on them suggested that their onset electronic transition showed a mixed character of MLCT and LLCT, which was consistent with literature case. In this case, the correlation between diamine ligand structure and $[Cu(N—N)(PPh_3)_2]$ photophysical performance was carefully checked. Detailed analysis on photophysical parameters suggested that the absorption edge of $[Cu(N—N)(PPh_3)_2]BF_4$ complex was controlled by diamine conjugation length. A wide absorption edge needed a short conjugation chain in diamine ligand. Similar tendency was found for their emission spectra. In addition, a long conjugation chain in diamine ligand widened emission spectra obviously. Emission dynamics showed slim correlation with diamine ligand conjugation length since the excited state was controlled mainly by dynamic procedure and steric factor of diamine ligands. This conclusion is expected to help further design for $[Cu(N—N)(PPh_3)_2]$ complexes with controllable optical edge. For later efforts, diamine ligands should be modified with bulky substituents so that the non-radiative decay procedure can be minimized, leading to improved PL performance.

Acknowledgments

The authors gratefully thank the financial supports of the NSFC (Grant No. 51572256) and the Science and Technology Innovation Fund Projects of Changchun University of Science and Technology (No. XJJLG-2016-04).

References

[1] M.W. Mara, K.A. Fransted, L.X. Chen, Coord. Chem. Rev. 282–283 (2015) 2–18.
[2] F. Dumur, Org. Electron. 21 (2015) 27–39.
[3] C.E. Housecroft, E.C. Constable, Chem. Soc. Rev. 44 (2015) 8386–8398.
[4] Y. Zhang, M. Schulz, M.W. chltler, M. Karnahl, B. Dietzek, Coord. Chem. Rev. 356 (2018) 127–146.
[5] D.G. Cuttell, S.-M. Kuang, P.E. Fanwick, D.R. McMillin, R.A. Walton, J. Am. Chem. Soc. 124 (2002) 6–7.
[6] S.M. Kuang, D.G. Cuttell, D.R. McMillin, P.E. Fanwick, R.A. Walton, Inorg. Chem. 41 (2002) 3313–3322.
[7] E. Leoni, J. Mohanraj, M. Holler, M. Mohankumar, I. Nierengarten, F. Monti, A. Sournia-Saquet, B. Delavaux-Nicot, J.-F. Nierengarten, N. Armaroli, Inorg. Chem. 57 (2018) 15537–15549.
[8] L. Yang, J.K. Feng, A.M. Ren, M. Zhang, Y.G. Ma, X.D. Liu, Chem. Eur. J. 10 (2005) 1867–1879.
[9] Q. Zhang, Q. Zhou, Y. Cheng, L. Wang, D. Ma, X. Jing, F. Wang, Adv. Mater. 16 (2004) 432–436.
[10] L. Zhang, B. Li, Z. Su, Langmuir 25 (2009) 2068–2074.
[11] A.R. Cabrera, I.A. Gonzalez, D. Cores-Arriagada, M. Natali, H. Berke, C.G. Daniliuc, M.B. Camarada, A. Toro-Labbe, R.S. Rojas, C.O. Salas, RSC Adv. 6 (2016) 5141–5153.
[12] L. Shen, X.L. Ding, T.F. He, X.L. Hao, J.F. Guo, L.Y. Zou, A.M. Ren, New J. Chem. 42 (2018) 3660–3670.

[13] M. Alkan-Zambada, S. Keller, L. Martinez-Sarti, A. Prescimone, J.M. Junquera-Hernandez, E.C. Constable, H.J. Bolink, M. Sessolo, E. Orti, C.E. Housecroft, J. Mater. Chem. C 6 (2018) 8460–8471.
[14] S. Keller, A. Prescimone, H. Bolink, M. Sessolo, G. Longo, L. Martinez-Sarti, J.M. Junquera-Hernandez, E.C. Constable, E. Orti, C.E. Housecroft, Dalton Trans. 47 (2018) 14263–14276.
[15] F. Brunner, A. Babaei, A. Pertegas, J.M. Junquera-Hernandez, A. Prescimone, E.C. Constable, H.J. Bolink, M. Sessolo, E. Orti, C.E. Housecroft, Dalton Trans. 48 (2019) 446–460.
[16] B. Chodhury, D. Mallick, K.K. Sarkar, K. Naskar, C. Sinha, Inorg. Chim. Acta 488 (2019) 125–130.
[17] R. Giereth, I. Reim, W. Frey, H. Junge, S. Tschierlei, M. Karnahl, Sustainable Energy Fules 3 (2019) 692–700.
[18] L. Zhang, B. Li, Z. Su, J. Phys. Chem. C 113 (2009) 13968–13973.
[19] L. Zhang, B. Li, L. Zhang, Z. Su, ACS Appl. Mater. Interfaces 1 (2009) 1852–1855.
[20] M.A. Baldo, C. Adachi, S.R. Forrest, Phys. Rev. B 62 (2000) 10967–10977.
[21] P. Chen, L. Zhao, Y. Duan, Y. Zhao, W. Xie, G. Xie, S. Liu, L. Zhang, B. Li, J. Lumin. 2001, 131, 2144–2147.
[22] L. Zhang, S. Yue, B. Li, D. Fan, Inorg. Chim. Acta 384 (2012) 225–232.
[23] L. Chen, S. Sun, J. Li, Z. Fang, Inorg. Chim. Acta 446 (2016) 24–31.